Available online at www.sciencedirect.com
SCIENCE DIRECT®

Ultramicroscopy 101 (2004) 183–195

ultramicroscopy

www.elsevier.com/locate/ultramic

Electron-acoustic and surface electron beam induced voltage signal formation in scanning electron microscopy analysis of semiconducting samples

W.K. Wong[a,*], E.I. Rau[b], J.T.L. Thong[a]

[a]*Department of Electrical & Computer Engineering, National University of Singapore, 4 Engineering Drive 3, Singapore 117576, Singapore*
[b]*Moscow State University and Institute of Microelectronics Technology of the Russian Academy of Science, Russia*

Received 15 October 2003; received in revised form 18 May 2004; accepted 15 June 2004

Abstract

The conditions for the detection of electron-acoustic (EA) and surface electron beam induced voltage (SEBIV) signals using a common sample mount and bottomside detection scheme are hereby discussed. It is shown that while the intrinsic properties of the sample under electron-beam irradiation would chiefly determine the presence of these contrast mechanisms, the manner in which the sample is mechanically and electrically configured in relation to the signal detection is crucial in determining the actual signal coupling mechanisms at work and hence the assumptions by which a robust and consistent interpretation of experimental results can be made. EA signals are detectable only if electrical coupling between the sample and the detector is defeated, a necessary pre-requisite as the signal magnitude of carrier-generated SEBIV coupling is 2–3 orders larger in most cases. With regards to SEBIV detection, bottomside SEBIV detection may be preferable to topside detection owing to minimization of topographic signal contribution, higher signal coupling efficiency and a less complex sample-detector mounting procedure.

PACS: 07.78.+s; 68.37.Hk; 41.75.Fr; 43.60.Lq

Keywords: SEAM; SEBIV; EBIC; Electron-acoustic; Capacitive-coupling

1. Introduction

Among the relatively newer and lesser-known methods particularly for the analysis of semiconducting samples in the Scanning Electron Microscope are the surface electron beam induced voltage (SEBIV) [1–3] and scanning electron acoustic microscopy (SEAM) [6,7] techniques. The parallels between the SEBIV technique and the family of electron beam induced current (EBIC), for both steady-state [4] and strobed

---

[*] Corresponding author. Tel.: +65-6874-2086; fax: +65-6779-1103.
E-mail address: elewwk@nus.edu.sg (W.K. Wong).

0304-3991/$ - see front matter © 2004 Elsevier B.V. All rights reserved.
doi:10.1016/j.ultramic.2004.06.002

modes including the single-contact pulsed mode [5] have been previously described and studied elsewhere in the context of their utility in the measurement of minority carrier diffusion length and lifetime quantification [8]. The SEAM technique was originally thought of as a mutually exclusive technique for the detection of acoustically coupled electrostriction phenomenon during the recombination of excess carriers as a semiconducting sample is irradiated by an electron beam [9], in addition to the other coupling mechanisms such as thermal-wave and piezoelectric coupling [10,11]. In this paper, the insights from recent work on the study of experimental conditions and detection properties of capacitively coupled bottomside detection of SEBIV and SEAM signals in a common detection configuration are presented. It will be shown that the intricacies of the detection configuration play a vital part in determining the degree to which these two signals can be discriminated depending on the electron beam-sample induced charge dynamics and the electrical configuration of a substrate-based acoustic detection scheme. The results of bottomside or backside SEBIV and SEAM detection will be compared with the topside SEBIV detection to highlight the relative properties of these two modes of detection.

The next two sections will describe the fundamental operating principles for SEBIV and SEAM while a common detection configuration for both these techniques will be presented in Section 4.

2. Principle of detection: SEBIV

The SEBIV mode involves the detection of variations in the surface potential that arise during the irradiation of a semiconducting material by an electron beam. In this application, electron–hole pair carriers are generated which subsequently results in a transient voltage generation on the surface of the sample due to carrier separation under a locally induced electric field across a depletion or space-charge region (SCR) as shown in Fig. 1. The charge dynamics in the sample are identical to the EBIC family and hence charge generation and recombination parameters such as minority carrier lifetimes and diffusion lengths can be studied using the detection of this induced voltage signal [8].

Two detection configurations for SEBIV can be used: Detection from the topside or alternatively, through the backside or substrate (see Fig. 1). In topside detection, the sample substrate is ohmically grounded through the substrate metal contact M2 with the dielectric layer D above M2 omitted, the topside metal contact M1 is floated (unconnected) and a metal ring electrode R with a typical diameter of 2–3 mm depending on the desired field of view is positioned close to

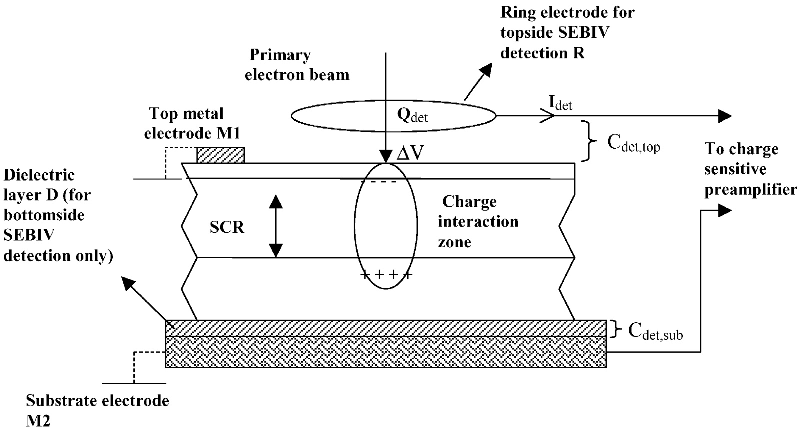

Fig. 1. SEBIV signal generation and detection.

the sample surface (typical electrode to sample separation is about 0.5 mm). The ring detector and sample surface form an electrostatic capacitor with capacity $C_{\mathrm{det,top}}$. By means of this capacitor arrangement a local potential ΔV at the specimen surface induces an image charge Q_{det} on the metal electrode, resulting in a transient displacement current $I_{\mathrm{det}} = \mathrm{d}Q_{\mathrm{det}}/\mathrm{d}t$ in the ring detector sub-circuit, where $\mathrm{d}t$ is the transient time corresponding to the charge change $\mathrm{d}Q_{\mathrm{det}}$. I_{det} can be amplified by a current to voltage preamplifier for subsequent signal acquisition and display on the SEM.

The bottomside detection scheme works on the same principle, except that the detection configuration is inverted with the metal contact M1 being grounded while the metal contact M2 serves as the capacitive pickup through the dielectric layer D. The ring electrode R is not used in this case. This method of detection is superior to the former detection configuration as the magnitude of the signal increases significantly due to the higher dielectric permittivity and also the larger bottomside detector area and hence capacitance of the substrate dielectric, $C_{\mathrm{det,sub}}$. For example, typical values for $C_{\mathrm{det,top}}$ and $C_{\mathrm{det,sub}}$ are 0.5 and 90 pF for a 1 mm loop in free space and a 16 mm diameter, 1 mm thick lead zirconate titanate (PZT) disc (also used for electron-acoustic (EA) detection as discussed later in greater detail in Section 3), respectively. In addition, spurious pickup from secondary and backscattered electrons (BSEs) is negated in bottomside detection, hence giving a purer SEBIV signal compared to topside detection. Sample-detector mounting is also much more straightforward in bottomside detection, compared to the additional effort required in precisely positioning the topside loop detector for optimal topside SEBIV signal coupling.

It was previously shown [1,2,8] that for top and bottomside SEBIV detection, the maximum magnitude of the detected SEBIV signal $\Delta V_{\max}$ in a p–n junction can be represented by the expression

$$\pm\Delta V_{\max} = C_{\mathrm{ef}}\beta \ln[1 + (G_0 I_0/I_s)], \tag{1}$$

where C_{ef} is the dimensionless capacitive coupling coefficient for the detector given by $C_{\mathrm{ef}} = C_{\mathrm{det}}/C_{\mathrm{i}}$, where C_{det} is the capacitance between the detector electrode and the irradiated surface area of the specimen and C_{i} the input capacitance of the charge preamplifier, $\beta = kT/q$ is the thermal potential, $G_0 = (E_0/E_{\mathrm{eh}})(1 - \Phi)$ is the generation rate of excess charge carriers, E_0 is the energy of primary electrons, E_{eh} is the energy needed for generation of an electron–hole pair, Φ is the fractional BSE energy defined as $\Phi = \eta\langle E\rangle/E_0$, where η is the BSE yield coefficient and $\langle E \rangle$ the mean BSE energy, I_0 is the primary electron beam current and I_s the reverse saturation current of the p–n junction.

If the sample is a semiconductor wafer with subsurface SCR, i.e. subsurface potential barrier without the presence of a p–n junction, then the maximum magnitude of the detected SEBIV signal $\Delta V_{\max}$ can be expressed as

$$\pm\Delta V_{\max} = C_{\mathrm{ef}}\beta \ln[1 + (\Delta n/N_0)], \tag{2}$$

where Δn and N_0 are the concentrations of the non-equilibrium and majority charge carriers, respectively.

The "+" sign in expressions (1) and (2) corresponds to the surface depletion layer (or to the layer with a slight inversion) for an n-type region, whereas the "−" sign corresponds to the same for the p-type.

As can be seen from Eqs. (1) and (2), an important parameter for the experimental detectability of SEBIV signals is the capacitive coupling coefficient for the detector, C_{ef}, with a larger value of C_{ef} resulting in a higher coupled signal magnitude. In practice, C_{det} and hence C_{ef} can be increased by decreasing electrode to sample separation, or by increasing the dielectric permittivity as in the case of bottomside detection as mentioned earlier. The relative sensitivity of SEBIV detection from the top and bottomside will be experimentally studied in Sections 4 and 5.

3. Principle of detection: scanning electron acoustic microscopy

SEAM was first reported in 1980 and involves the detection of transient acoustically coupled thermal waves in the SEM [13,14]. Owing to sensitivity considerations, primary electron beam pulsing in conjunction with lock-in amplification is commonly employed to attain higher signal-to-noise performance. As the pulsed electron beam is scanned across the semiconductor surface, energy is absorbed within the sample bulk, causing local periodic heating and resulting in local crystallographic expansion and contraction (see Fig. 2). Highly damped thermal waves are generated as a result and their propagation are mostly limited to within a thermal wavelength, μ, given by the relationship

$$\mu = (2K/\rho C\omega)^{1/2}, \tag{3}$$

where K is the thermal conductivity of the material, ρ the density of the material, C the specific heat and ω the angular modulation frequency. Example values of μ for some common materials and frequency dependence are given in Table 1.

Thermal waves introduce stress–strain conditions on the lattice structure and ultimately result in phonons or acoustic waves being generated and propagated through the material, where they can be detected using suitable acoustic to electric transducer configurations. In general, EA signal detection can be accomplished either by surface (shear) or bulk wave phonon detection. In this study, the latter detection mode will be studied due to the common detector configuration between this and the bottomside SEBIV detection technique.

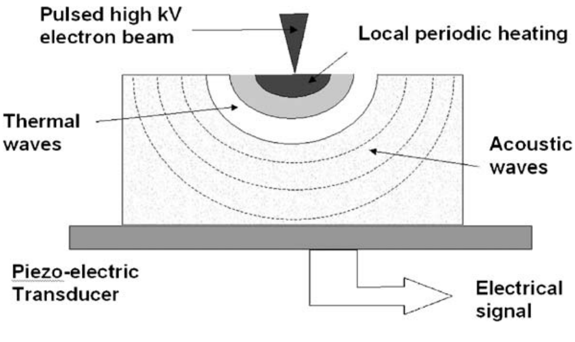

Fig. 2. EA signal formation under the thermal-wave mechanism.

Table 1
Examples of thermal diffusion lengths

Material	Thermal diffusion length, μ (μm)	
	at 50 kHz	at 1 MHz
Silicon	53.7	12.0
Organic coating	4.5	1.0
Aluminum	13.4	3.0

The signal contrast mechanism in SEAM under the thermal-wave mechanism is therefore dependent on thermal-elastic characteristics of the sample, while the spatial resolution D is determined by the following relation:

$$D(= d_b^2 + R_0^2 + \mu^2)^{1/2}, \tag{4}$$

where d_b is the electron beam diameter and R_0 the generation volume diameter (the electron path length) [6]. The amplitude of the thermal-acoustic signal is given by the expression

$$A = \alpha BQ/(\omega\rho CK)^{1/2}, \tag{5}$$

where α is the coefficient of thermal expansion of the material, B the bulk modulus of elasticity (reduced Young's modulus) and Q the heat source power. In reality, EA signal generation is a relatively inefficient process owing to: (i) The multiple energy-conversion steps from the kinetic energy of the primary electrons to the final acoustic wave generation; (ii) The effect of acoustic damping of the sample and sample holder bulk and; (iii) Lossy acoustic coupling due to surface imperfections and acoustic impedance mismatch at the various interfaces between the sample and the transducer. In practice, probe power in excess of a few milliwatts is commonly required for adequate final EA detection performance where the thermal-wave mechanism is involved.

In addition to thermal-acoustic generation discussed so far, other phonon-generation mechanisms in EA detection have also been proposed, for example, ferroelectric contrast [10], excess carrier recombination [12], internally generated space charges in semiconductors and dielectrics [15] leading to the additional mechanisms of local piezoelectricity and electrostriction [16], magneto-elastic interactions in ferromagnetic samples [17] and photostrictive mechanisms [18]. The presence or absence of these mechanisms is extremely specific on the sample and detector configuration; hence analysis of EA results has to be done in the context of each of these contrast mechanisms.

Although the SEBIV and SEAM techniques have been discussed separately so far, they share a common detector configuration as far as sample bottomside detection is concerned. The following sections will discuss the experimental configuration and procedure for SEBIV and EA detection in a common detection setup.

4. Experiment for concurrent SEBIV and EA detection

The setup shown in the overall system block diagram of Fig. 3 was used to study the conditions for the acquisition of SEBIV and EA-type signals. The SEM used was a Hitachi S-2700 fitted with a LaB_6 thermionic emission gun equipped with a beam blanker. The LaB_6 gun gives a high beam current that is necessary particularly for EA signal detection as previously mentioned. A typical maximum beam current of about 2 μA at a beam energy of 25 keV provides more than sufficient margin for EA detection. The signal outputs from the SEBIV and EA detectors are routed through a preamplifier and also a lock-in amplification stage in the case of strobed mode operation using a pulsed primary beam. A PC is used for digitally controlled beam scanning and signal acquisition.

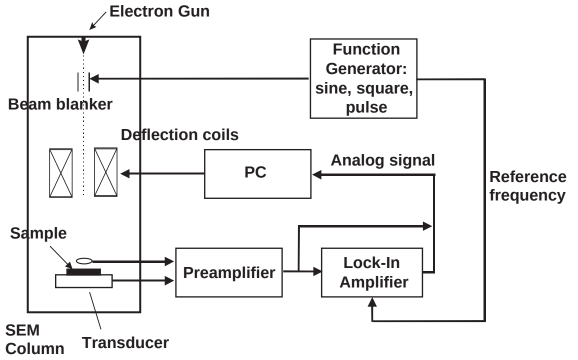

Fig. 3. Overall system configuration for concurrent EA and SEBIV detection.

The detector module shown in Fig. 4 forms the sample-piezoelectric transducer module shown in the overall system schematic of Fig. 3, and is the experimental realization of the setup shown in Fig. 1. The device-under-test (DUT) (1) forms the topmost layer of a detection stack consisting of a piezoelectric or dielectric element that is metallized on both faces for ohmic contact (2) and an acoustically reflective tungsten spacer (3) that serves both to confine acoustic waves for higher detection amplitude response as well as to serve as an electrical signal feedthrough (6). The stack is housed in an electrically conductive shell (5) that is electrically insulated (4) from the detection stack. In the configuration of Fig. 4(a), the piezoelectric/dielectric element (2) is electrically grounded on the top surface at the sample substrate. Therefore, electrical coupling through the sample substrate is eliminated and only phonon-based piezoelectric (EA) coupling is present in this configuration. In Fig. 4(b), the grounding point resides at the sample surface. Given the considerable resistance present between the sample surface and the sample bottomside, both electrical and phonon coupling is present in this configuration, enabling both SEBIV and EA signals to be detected. The SEBIV selectivity achieved by alternating between these two configurations can therefore be utilized to study the properties of SEBIV and EA detection in a common substrate-based detector.

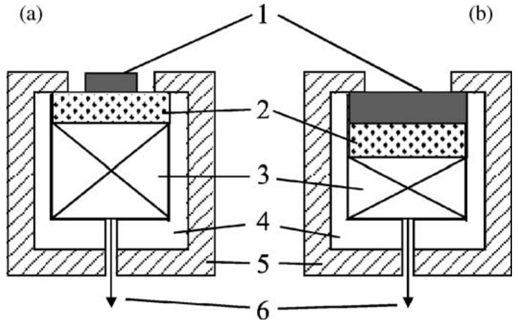

Fig. 4. Sample mounting configuration used for the p-doped Si sample where (a) The piezoelectric/dielectric (PZT/SiO_2) disc is grounded directly; (b) Grounding point located on the topside of sample. Configuration of sample holder showing (1) Sample; (2) Piezoelectric/dielectric disc; (3) Electrically conducting tungsten spacer; (4) Electrically insulating spacer; (5) External ground shell; and (6) Electrical signal feedthrough.

Two samples were chosen for the studies, the first being an Si sample with selectively p-doped regions, and the second being a bipolar junction transistor (BJT) array (Harris' CA3096) consisting of three npn and two pnp transistors in one DIP package. The five BJTs of the CA3096 provide a sufficient number of permutations of p–n junctions for this study. A PZT transducer[1] was used as the piezoelectric element. Using a PZT, both acoustic and electrically coupled signals can be derived. Alternatively, an SiO_2 disc was used as a substitute for the PZT to exclude piezoelectricity and hence acoustic coupling, thus forming the purely electrical or SEBIV detection mode through the substrate.

Two probe modulation schemes were studied: The first uses a continuous scanned beam, and the second utilizes beam blanking for probe beam amplitude modulation. For the modulated primary beam experiments, the detector output signals were routed through an additional lock-in amplification stage.

5. Results and discussion

5.1. Topside SEBIV detection in p-doped Si test sample

Detection of SEBIV signals from the topside was extensively described in previous publications [1–3,8] and is hereby used as the reference experimental set in order to compare the characteristics of bottomside SEBIV and SEAM detection. Topside SEBIV experiments were performed using a metallized Si sample with p-doped regions. The oxide and aluminum metallization on the left half of the area depicted in Fig. 5(a) have been etched away, leaving only the underlying doped Si regions. The oxide and metallization on the right half were left intact. A 25 keV electron beam with a probe current of about 10 nA on the Hitachi S-2700 LaB_6 SEM was used in most cases, except for EA detection where beam currents of about 1 μA were used. SEBIV images were obtained using a continuous beam (Fig. 5(b)) and with beam-pulsing and lock-in signal amplification (Fig. 5(c)). In the former, the displacement currents (I_{det}) were generated mainly due to the modulation of the signal as electron beam is scanned across doping boundaries. As the beam is scanned in a raster with the scan rate in the x-direction being about 500 × higher than the y-direction, the resultant image contrast is obtained primarily along the doping boundaries normal to x, i.e. the vertical edges as seen in Fig. 5(b). However, when beam-pulsing of 10 kHz together with lock-in amplification is used, and with the x-scan being set at a much lower rate than the beam-pulsing rate to allow for sufficient lock-in sampling at a given pixel, image contrast is obtained along both x- and y-axes as shown in Fig. 5(c). The differing contrast properties obtained using these two detection schemes have been termed "edge contrast" and "area contrast", respectively [19]. In either case, the results show that image contrast corresponding to the different levels of doping in the Si test sample can be obtained using capacitively coupled topside SEBIV detection. From a qualitative examination of the results, it is observed that the resolution of SEBIV imaging is mostly limited by nonequilibrium carrier diffusion length [8] and therefore is similar to the resolution attainable by the EBIC technique.

Figs. 5(b) and (c) also reveal that there is a small amount of topography present in the topside SEBIV images due to the contribution of sample-emitted electrons hitting the loop detector; bottomside detection through the sample substrate may be preferable when total rejection of emitted electrons is desired [2]. Another advantage of substrate detection is the higher signal sensitivity due to the inherently larger dielectric permittivity of the substrate dielectric compared to the free space between the topside loop detector and the sample.

5.2. Through-substrate SEBIV and EA detection in p-doped Si test sample

The sample previously used for topside SEBIV detection was reconfigured for bottomside EA detection configuration as described earlier in Section 4; the resultant images are shown in

---

[1] Morgan Matroc Ceramic's PZT-5B.

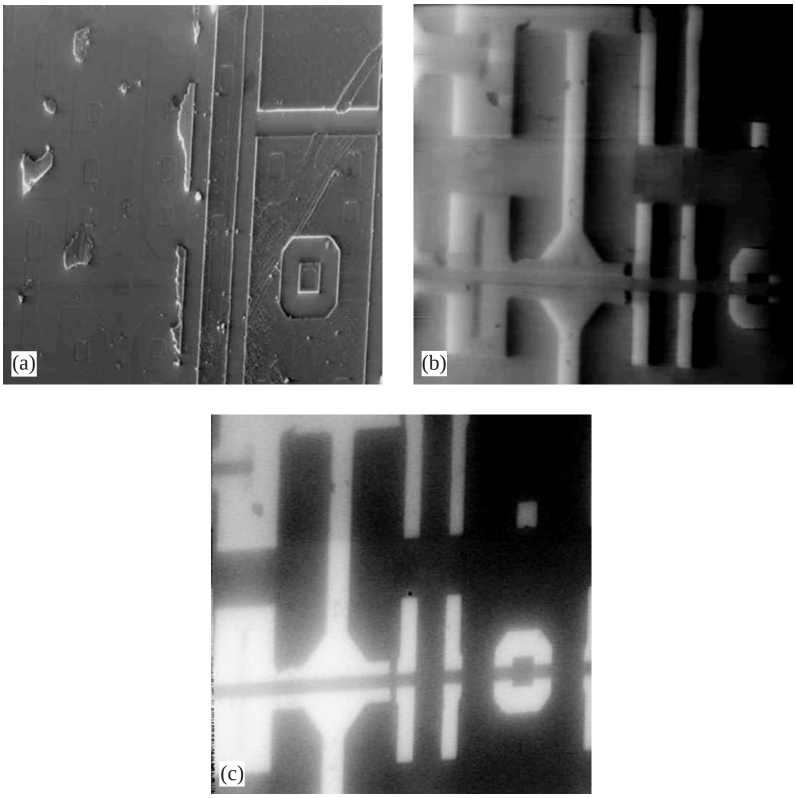

Fig. 5. Micrographs showing (a) SE image of doped Si test sample; (b) Topside SEBIV detection without beam modulation; (c) Topside SEBIV detection with beam pulsing at 10 kHz. Scan width = 500 μm.

Figs. 6(a)–(c). Fig. 6(b) shows the specimen or absorbed current image which serves as a control case to evaluate the contribution of bulk currents on EA and SEBIV signal detection from the bottomside. As expected, only topographical contrast is obtained in both the SE (Fig. 6(a)) and specimen current images. Fig. 6(c) shows an EA image of the sample obtained at a probe current of about 1 μA using the detection configuration of Fig. 4(a), i.e. when the sample is grounded from the backside and consequently at the top surface of the PZT. Since the grounding surface shields the electrically coupled signals from the PZT, no SEBIV coupling through the sample substrate is obtained. Instead, the EA image of Fig. 6(c) acquired at one of the detection resonance points of 113 kHz shows contrast originating from electron–acoustic interaction, with the contrast being determined by differences in material and hence acoustic impedances instead of electron emission properties, with the Al metallization regions having the highest EA signal levels. Also, the resolution obtained from EA detection is much poorer compared to the SE, specimen current and SEBIV images for a given set of probe beam parameters as can be observed from Figs. 5 and 6. The theoretical resolution for SEAM imaging of Si at 113 kHz is calculated to be about 35.7 μm using Eqs. (3) and (4), with the thermal wavelength μ being the dominant resolution parameter. This fact, together with the multi-resonant frequency characteristics of the signal detection in this configuration, confirms that the EA mechanism dominates for the sample-detector configuration of Fig. 4(a).

The above-mentioned high probe currents (1 μA) required for EA imaging exemplify the relatively poor efficiency of acoustic signal generation in

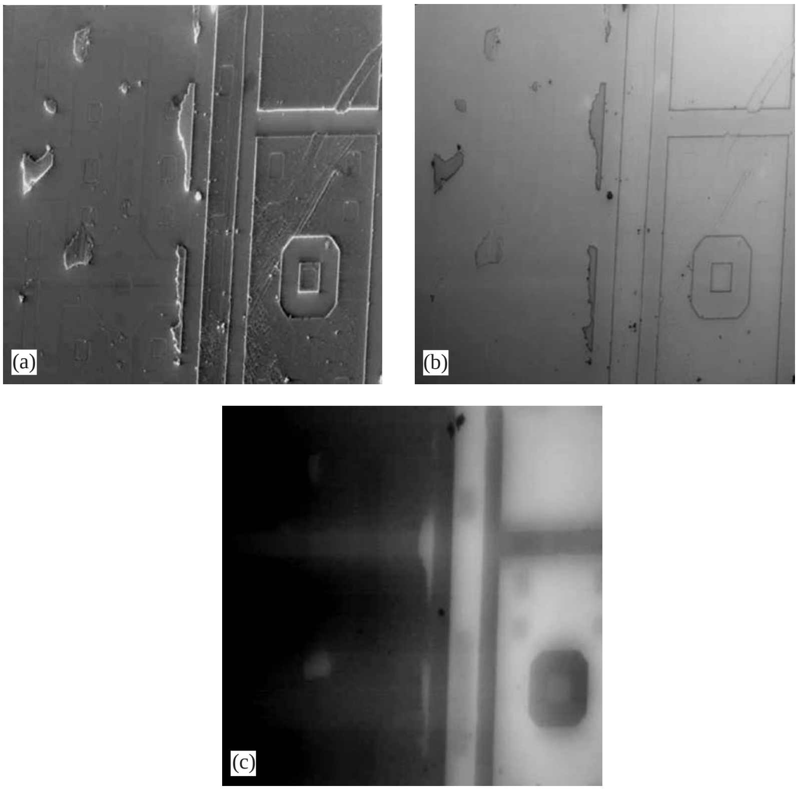

Fig. 6. Micrographs showing (a) SE topography; (b) Specimen current image; (c) Using PZT transducer (EA detection mode) at 113 kHz (resonant peak) with grounding configuration shown in 4(a). Scan width = 500 μm.

SEAM, which requires 2–3 orders of magnitude higher probe currents compared to charge collection techniques such as EBIC and SEBIV to achieve reasonable image quality; this point has been attributed to the inefficient nature of the multiple energy conversion steps involved in EA detection and also losses due to acoustic damping in the detection stack [6]. On the other hand, the electron–hole pair generation process in SEBIV and EBIC detection is much more efficient, with probe to junction current multiplication factors of the order of thousands easily attainable in EBIC.

From the configuration shown in Fig. 4(a), the grounding configuration was changed to that described in Fig. 4(b), with the signal ground now being connected to the topside of the sample instead of the topside of the PZT transducer, which is now electrically floating at a finite resistance of a few kilo ohms from ground imposed by the conductivity of the test sample. In this case, any electrical potential due to SEBIV at the sample would be coupled through the sample substrate. This is evidenced by the images obtained using bottomside detection, and still using the PZT as the substrate dielectric, as shown in Fig. 7(a) (without modulating the beam) and Fig. 7(b) (with the beam modulated at the frequency of 200 kHz), which reveals a marked departure from the EA-dominated contrast of Fig. 6(c). Firstly, the contrast characteristics closely resemble that of the topside SEBIV detection mode shown in Figs. 5(b) and (c). Subsequent substitution of the piezoelectric PZT transducer with non-piezoelectric dielectric discs such as phosphosilicate glass (PSG), Teflon™ and SiO_2 did not fundamentally alter the contrast properties of the images obtained from that of Figs. 7(a) and (b). Secondly, the contrast characteristics exhibit a wideband and comparatively

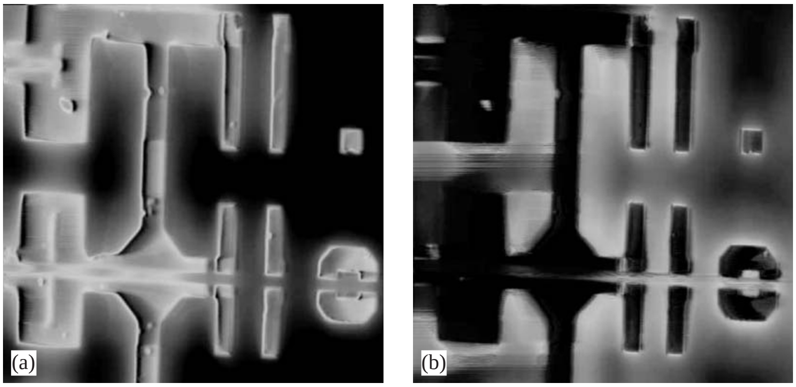

Fig. 7. (a) Bottomside detection without beam modulation; (b) Bottomside detection with beam pulsing at 200 kHz. Grounding configuration shown in 4(b) was used. Dominant signal generation mechanism is SEBIV and not EA. Scan width = 500 μm.

flat amplitude response as a function of frequency, a departure from the resonant behaviour that is characteristic of acoustic coupling. Thirdly, the transducer electrical signal levels were also between 2 and 3 orders of magnitude stronger than the EA mode for a given probe current, with sufficient signal modulation obtained even without beam blanking and lock-in amplification (Fig. 7(a)) that is absolutely required for sufficient EA detectability.

From these observations, it can be concluded that the dominant signal generation mechanism for semiconducting samples with the mounting configuration of Fig. 4(b) is electrically coupled SEBIV, even when a piezoelectric transducer is used. This outcome highlights the importance of the sample-detector mounting configuration, particularly the electrical grounding of the transducer and sample when performing EA detection through the substrate for semiconducting samples. Particular care in ensuring adequate electrical grounding must be taken to minimize the possibility of electrical coupling through the piezoelectric transducer so as to negate the possibility of detection of SEBIV signals, especially as the signal generation efficiency in EBIC-type mechanisms is a few order of magnitudes higher than the thermal-wave mechanism in EA detection.

One final point is that bottomside SEBIV detection generally exhibits reduced topographical artifacts from background emitted electron pickup compared to topside detection. This property may be advantageous in certain applications where a purer image of doped regions without interference from surface topography is required. An exception to this lies in situations where the sample morphology is such that the beam-landing characteristic at the sample surface is significantly affected as can be seen from the effect of particulates on the surface of the doped Si sample on the bottomside SEBIV image contrast (Figs. 7(a) and (b)).

5.3. SEBIV and EBIC analysis of CA3096 bipolar transistor array

An experiment to compare the characteristics of SEBIV and EBIC detection was carried out using the CA3096 transistor array, which consists of three npn and two pnp BJTs. This sample was selected as a representative example of a more realistic application for the analysis of p–n junctions given the larger but still manageable number of p–n junction configurations that the CA3096 provides. Several images were obtained using the mounting scheme of Fig. 4(b) using both topside and bottomside SEBIV detection. The primary beam landing energy used is 20 keV and the primary probe current is set to approximately 5 nA on a Hitachi S-3500N tungsten source SEM. To exclude EA coupling through the substrate, a dielectric SiO_2 disc is used as the capacitive element. Images of two selected transistors using

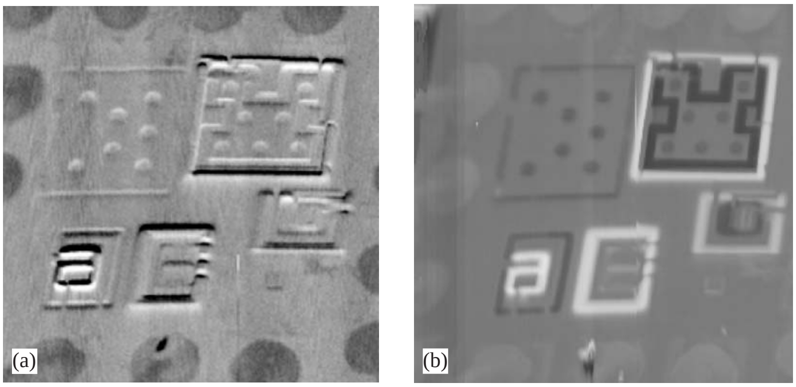

Fig. 8. SEBIV topside detection showing: (a) Unmodulated beam (edge contrast); and (b) With lock in detection at 2 kHz (area contrast). Scan width = 680 μm.

the established EBIC method across the emitter and substrate of the device were also obtained to serve as the reference charge collection results. Five experimental configurations were studied and the resultant micrographs obtained are as follows:

1. Topside SEBIV, without beam modulation (Fig. 8(a))
2. Topside SEBIV, with beam modulation and lock-in amplification at 2 kHz (Fig. 8(b))
3. Bottomside SEBIV, without beam modulation (Fig. 9)
4. Bottomside SEBIV, with beam modulation and lock-in amplification at 2 kHz (Fig. 10)
5. EBIC micrographs across emitter-substrate of selected npn and pnp transistors (Fig. 11).

Note that the images in Figs. 8 and 9 have been rotated through 90° relative to the SEM raster scanning axes; the higher scan rate of the raster is therefore in the y-direction, yielding stronger edge contrast features on horizontal edges when looking at the unmodulated primary beam SEBIV images shown in Figs. 8(a) and 9. The contrast characteristics obtained here are consistent with the edge contrast obtained using the doped Si test sample described in the last section. Similarly, employing a pulsed primary electron beam and lock-in amplification yields an area-type contrast of the p–n junctions of the BJT as shown in Figs. 8(b) and 10. Comparing the topside (Figs. 8(a) and (b)) and bottomside SEBIV detection (Figs. 9 and 10) cases, it is again observed that the signal levels for bottomside SEBIV detection are noticeably higher as indicated by the lock-in amplifier gain settings than that from the topside, as predicted by Eqs. (1) and (2) due to the larger capacitance of the dielectric.

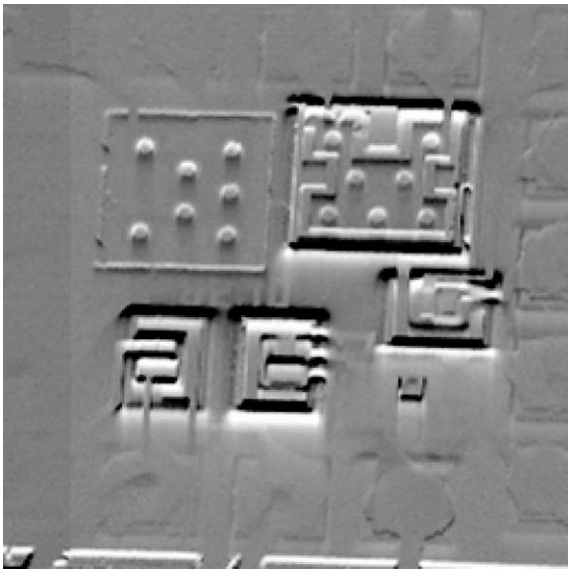

Fig. 9. Bottomside SEBIV detection, edge contrast using unmodulated primary electron beam. Scan width = 680 μm.

Closer examination of these results and also that of SEBIV detection from the bottomside of the sample using beam modulation (Fig. 10) shows that in a more complex sample such as the CA3096 with multiple p–n junctions, not all of the

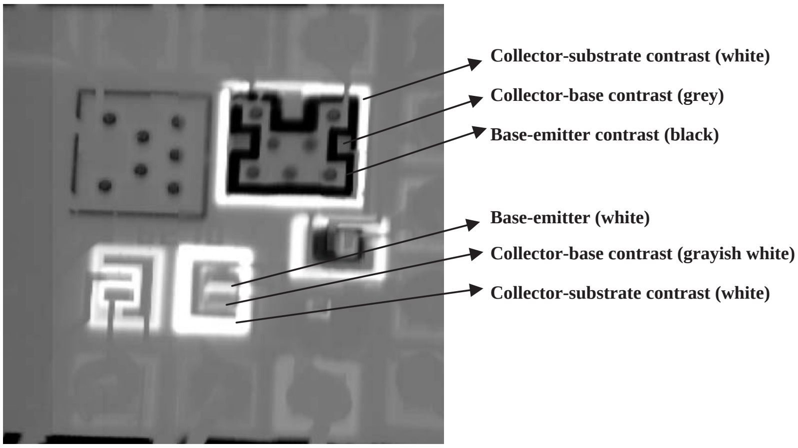

Fig. 10. Bottomside SEBIV detection, with lock in detection at 2 kHz (area contrast) and showing BJT p–n junction zones. Scan width = 680 μm.

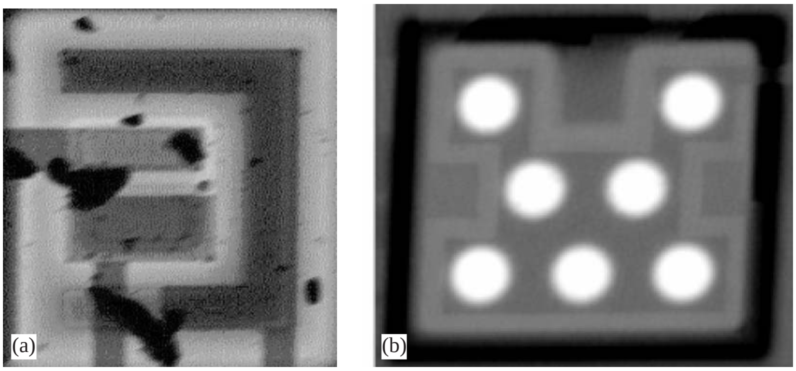

Fig. 11. EBIC micrograph across emitter-substrate of: (a) bottom-left npn (scan width = 150 μm); and (b) top-right pnp (scan width = 250 μm).

junctions are equally well-detected using SEBIV, whether from the topside or bottomside. For example, junction contrast from the top-left pnp transistor is not as pronounced as the other BJTs, for both edge and area contrast imaging modes. It is suspected that the geometric configuration or layout of the pnp regions and metallization layers of this particular BJT are responsible for this behaviour, which ultimately results in a significantly reduced final capacitive signal coupling from the BJT in question. This was substantiated by experiments using EBIC which showed that standard EBIC contrast was obtainable from the said BJT, thus suggesting that the root cause is one of insufficient capacitive signal coupling and not of reduced electron–hole pair signal generation dynamics. The effect of sample structure on SEBIV detection efficiency is currently under study.

Comparing the results for SEBIV (Figs. 8–10) and that obtained for EBIC (Fig. 11) for two of the CA3096s BJTs reveal a high degree of correlation between the two detection methods, suggesting that the same underlying physics is responsible for signal formation. For example, the contrast characteristics for the npn BJT in the bottom left of Fig. 10 under SEBIV and in Fig. 11(a) under EBIC are identical except for the effect of primary beam shadowing due to subsequent surface dust particle contamination as seen in Fig. 11(a). The only difference lies in the inverted contrast for the top-right pnp transistor between SEBIV (Figs. 8(b) and 10) and EBIC (Fig. 11(b)), although the contrast properties across feature boundaries remain fundamentally identical. The contrast inversion is an instrumentation artifact of the lock-in amplification used for the beam-modulated area contrast SEBIV detection, which is dependent on the reference frequency used for a given experiment. Hence it is important to note the relative nature of image contrast interpretation in these two techniques. This point however, should not devalue their utility as far as the junction-mapping application is concerned.

Finally, with respect to the practicality of these two techniques, the following points can be made regarding two advantages of SEBIV over conventional EBIC:

(i) The elimination of the need to make external electrical contacts to specific nodes on the sample. This significantly simplifies the experimental setup whenever charge collection microscopy analysis is desired, and also relaxes the environmental constraints of implementing I/O in an evacuated specimen chamber.
(ii) Contrast can be obtained simultaneously from all junction areas on a sample in SEBIV detection in most cases, whereas contrast is obtained only from the immediate interconnected junction in EBIC. This parallel contrast acquisition greatly improves analysis throughput especially for samples with a large number of junctions as is common with the high device count of modern day VLSICs.

6. Conclusion

The results highlight the importance of sample-detector mounting configuration in determining whether acoustic or electrical coupling and hence EA or SEBIV contrast mechanisms dominate in the piezoelectric and capacitively coupled backside analysis of semiconducting samples. In all cases, EBIC-induced potentials generated in semiconductor structures tend to dominate over the thermal-acoustic (EA) response, which is significantly weaker. In the issue of topside vs. bottomside SEBIV detection, it is shown experimentally that bottomside detection gives a stronger contrast compared to topside SEBIV due to the higher detector capacitance as well as providing better rejection of topographical contrast. The contrast features for SEBIV have been shown to be highly correlated to EBIC, suggesting that the same fundamental charge dynamics are responsible for signal contrast. Hence, the SEBIV technique provides a superior charge collection experimental method especially as contrast is derived simultaneously from all junctions, whereas EBIC contrast is localized to the junction where the interconnections are made.

Acknowledgements

The authors would like to thank Prof. E. Plies (University of Tübingen, Germany) for providing the sample described in Figs. 5–7, and also Scanning Beam Technology Pte. Ltd. for providing the SEAM detection setup. The efforts of TE Teh and BS Lim are also acknowledged.

References

[1] V.A. Gostev, A.N. Zhukov, S.H. Moll, E.I. Rau, E.B. Yakimov, Bulletin of the Russian Academy of Sciences (Physics), vol. 62, Allerton Press Inc., New York, 1998, pp. 481.
[2] B. Degel, M. Kienle, E. Plies, E.I. Rau, S.Q. Zhu, Proceedings of EUREM XII, Brno, vol. III, Czechoslovakia, 2000, pp. 475.
[3] E.I. Rau, A.N. Zhukov, E.B. Yakimov, Solid-State Phenom. 63–64 (1998) 327.
[4] H.J. Leamy, J. Appl. Phys. 53 (1982) R51.
[5] S. Kolachina, J.C.H. Phang, D.S.H. Chan, Solid-State Electronics 42 (1998) 957.
[6] L. Balk, in: P.W. Hawkes (Ed.), Advances in Electronics and Electron Physics, vol. 71, Academic Press, Boston, 1988, p. 1.
[7] E. Brandis, A. Rosencwaig, Appl. Phys. Lett. 37 (1980) 98.
[8] S.Q. Zhu, E.I. Rau, F. Yang, Semiconductor Science and Technology 18 (2003) 361.
[9] M. Domnik, L.J. Balk, Scanning Microscopy 7 (1993) 37.
[10] W.K. Wong, Q.R. Yin, J.T.L. Thong, J.C.H. Phang, J.W. Fang, Proceedings of International Symposium for

Testing and Failure Analysis (ISTFA), Bellavue (Seattle), Washington, 2000 pp. 11.
[11] X.X. Liu, L.J. Balk, H.P. Abicht, A. Eckau, Q.R. Yin, Solid State Phenom. 63–64 (1998) 361.
[12] V.A. Sablikov, V.B. Sandomirskii, The photoacoustic effect in semiconductor, Phys. Stat. Sol. B (East Germany) 120 (1983) 471.
[13] E. Brandis, A. Rosencwaig, Appl. Phys. Lett. 37 (1980) 98.
[14] G.S. Cargill III, in: E. Ash (Ed.), Scanned Image Microscopy, Academic Press, New York, 1980, p. 319.
[15] M. Sasaki, H. Negishi, M. Inoue, J. Appl. Phys. 59 (1986) 796.
[16] N. Kultscher, L.J. Balk, J. Scanning Electronic. Micros. I (1986) 33.
[17] L.A. Koirakh, V.L. Preobrazhenskii, Sov. Phys. Acoust. 30 (1984) 134.
[18] R.G. Stearns, G.S. Kino, Appl. Phys. Lett. 47 (1985) 1048.
[19] Rau Detector Operating Manual. Raith Gmbh, Germany, 1989.